

REGULAR PAPER

Piezoelectric MEMS-based physical reservoir computing system without time-delayed feedback

To cite this article: Takeshi Yoshimura *et al* 2023 *Jpn. J. Appl. Phys.* **62** SM1013

View the [article online](#) for updates and enhancements.

You may also like

- [Characterization of Stable Fluorine-Doped Silicon Oxide Film Prepared by Biased Helicon Plasma Chemical Vapor Deposition](#)
Takahiro Tamura, Youichi Inoue, Makoto Satoh *et al.*
- [Electrochemical Formation of RE-Zn \(RE=Dy, Nd\) Alloys in a Molten LiCl-KCl System](#)
Hirokazu Konishi, Hideki Ono, Toshiyuki Nohira *et al.*
- [Improving the energy efficiency of using solar panels](#)
G V Nikitenko, E V Konoplev, V K Salpagarov *et al.*



Piezoelectric MEMS-based physical reservoir computing system without time-delayed feedback

Takeshi Yoshimura^{1*}, Taiki Haga¹, Norifumi Fujimura¹, Kensuke Kanda², and Isaku Kanno³

¹ Department of Physics and Electronics, Graduate School of Engineering, Osaka Metropolitan University, Sakai 599-8531, Japan

² Department of Electronics and Computer Science, Graduate School of Engineering, University of Hyogo, Himeji 671-2201, Japan

³ Department of Mechanical Engineering, Graduate School of Engineering, Kobe University, Kobe 657-8501, Japan

*E-mail: yoshimura@omu.ac.jp

Received June 3, 2023; revised July 5, 2023; accepted July 11, 2023; published online August 1, 2023

In this study, a physical reservoir computing system, a hardware-implemented neural network, was demonstrated using a piezoelectric MEMS resonator. The transient response of the resonator was used to incorporate short-term memory characteristics into the system, eliminating commonly used time-delayed feedback. In addition, the short-term memory characteristics were improved by introducing a delayed signal using a capacitance-resistor series circuit. A Pb(Zr,Ti)O₃-based piezoelectric MEMS resonator with a resonance frequency of 193.2 Hz was employed as an actual node, and computational performance was evaluated using a virtual node method. Benchmark tests using random binary data indicated that the system exhibited short-term memory characteristics for two previous data and nonlinearity. To obtain this level of performance, the data bit period must be longer than the time constant of the transient response of the resonator. These outcomes suggest the feasibility of MEMS sensors with machine-learning capability. © 2023 The Japan Society of Applied Physics

1. Introduction

The rapid development of artificial intelligence (AI) and machine learning has been driven by the emergence of neural networks that represent a model of neurons and their connections in the human brain. Recurrent neural networks (RNN) are deep learning network structures that use past information to improve network performance for current and future inputs. While RNN is commonly used in the analysis of time series data, such as speech recognition and natural language processing, increasing the number of neurons is necessary to improve performance, leading to a dramatic increase in computational load.

Reservoir computing (RC), a special model of RNN, has attracted much attention in recent years.¹⁾ A conceptual illustration of RC is shown in Fig. 1(a). The input data is linearly separated by projecting it onto a higher dimensional space with a nonlinear transformation, and only the output is used for learning. A more important feature of RC is that the nonlinear transformation part, called a reservoir layer, can be implemented in hardware using not only electrical charges and light, but also physical phenomena that are conventionally regarded as having little relation to computation. This paradigm is known as physical RC.^{2–8)} While current AI uses software-constructed neural networks and complex learning algorithms that require enormous amounts of computation, RC consumes orders of magnitude less computation and is expected to enable small, fast, and energy-efficient AI devices suitable for edge computing.

To realize high-performance physical RC, it is suggested that the reservoir layer consists of randomly connected nodes with slightly disparate properties.^{1–8)} For the nodes, physical phenomena with moderate nonlinearity and short-term memory properties are suitable. Ferroelectrics, which exhibit various nonlinearities in dielectric, optic, and electromechanical responses, seem to be attractive materials for physical RC.^{9–15)} Indeed, Toprasertpong et al. have demonstrated the physical RC system using ferroelectric gate FETs, in which hafnium zirconium oxide ferroelectric film was employed as the gate insulator of FET.^{16–18)} Using the rich dynamics

originating from ferroelectric polarization switching, computational tasks on time-series data processing, including nonlinear time series prediction, have been successfully solved.

We have developed piezoelectric MEMS resonators for vibration energy harvesting.^{19–21)} In addition to improving the characteristics of piezoelectric thin films including Pb(Zr,Ti)O₃,^{22,23)} (K,Na)NbO₃,²⁴⁾ and BiFeO₃,^{25–27)} the increase of the output power was investigated by devising device structures.^{28–30)} In the analytical model of the piezoelectric MEMS resonators, the mechanical domain is described by the Duffing equation, which is used to model nonlinear dynamic systems. This insight made us recognize that the piezoelectric MEMS resonator meets the requirements for physical RC. The high-quality factor resonators exhibit long transient responses at the resonance, which can be regarded as a short-term memory characteristic. In addition, resonators with large oscillations exhibit nonlinear resonance characteristics due to their materials and geometrical structures. Although the transient response of the MEMS resonators is rather slow, it appears to be closely matched to the speed of dynamic phenomena in the real environment. Thus, MEMS-based physical RC is expected to realize sensors with machine-learning functions.

A MEMS-based RC system was first demonstrated in 2018³¹⁾ and has been able to accurately emulate nonlinear dynamic tasks and compute the parity of random bit streams. Subsequently, various MEMS-based RC systems, including neuromorphic accelerometers, have been proposed.^{32–38)} To obtain sufficient short-term memory characteristics, most of these systems employ time-delayed feedback and additional masking procedures. In the former, the output from the reservoir layer is delayed for a certain period of time and then input to the reservoir layer again. This makes it possible to add short-term memory characteristics to the reservoir layer which does not have it. The latter is a pre-processing procedure to introduce a complex transient response. A temporal mask is applied to each input data as the weight between the input signal and the time-delayed feedback signal. Nondelay-based RC has been demonstrated using transient resonance and a Duffing nonlinear response in an

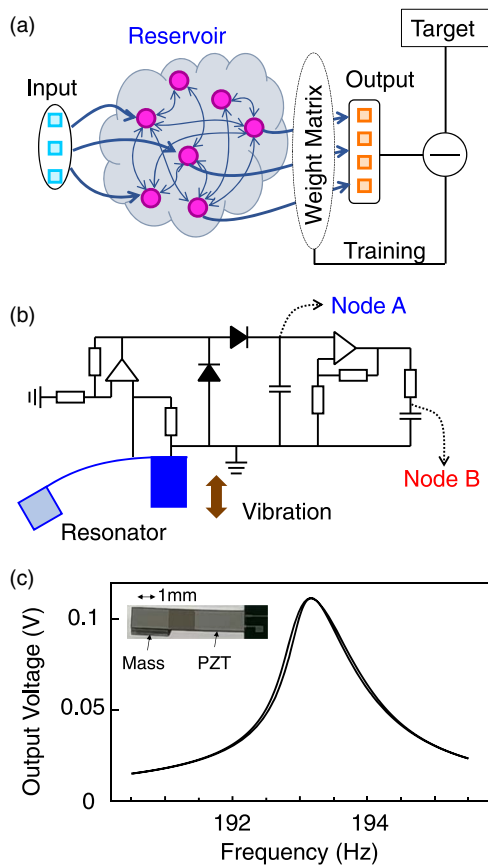


Fig. 1. (a) Conceptual illustration diagram of RC. (b) Circuit diagram of the piezoelectric MEMS RC system. (c) Frequency dependencies of the output voltage of the resonator. The inset represents the micrograph of the resonator.

electrostatic MEMS resonator.³⁹⁾ We investigated physical RC using piezoelectric MEMS resonators.⁴⁰⁾ In contrast to electrostatic MEMS, which require a voltage input to read the capacitance, the sensors using direct piezoelectric effect produce an output voltage simply by applying strain. Therefore, piezoelectric MEMS is expected to have advantages in the construction of RC systems with a large number of actual nodes. In this study, the potential of piezoelectric MEMS resonators as physical RC was investigated by employing the virtual node scheme that time-resolves the transient response of the resonator.

2. Principles and experiments

A circuit diagram of the piezoelectric MEMS RC system developed in this study is shown in Fig. 1(b). A single piezoelectric MEMS resonator, which works as an actual node, is oscillated by applying vibration. When the vibration frequency is close to the resonance frequency of the resonator, an AC signal with a transient response is generated. The output signal was amplified between 5 and 10 V by an operational amplifier and then rectified by diodes. This signal was denoted as Node A. It should be noted that this amplification is not necessary if the output signal from the resonator is sufficiently large. The signal of Node A was further amplified and input into a capacitor–resistor (CR) series circuit to generate a delay signal called Node B. The introduction of Node B is intended to improve short-term

memory performance. In addition, Node B is a linear mapping of Node A in the context of RC.

The resonator was fabricated through a conventional MEMS process using an SOI substrate. It has a simple cantilever structure with a length of 6 mm and a proof mass on the free ends. The micrograph of the resonator is shown in the inset of Fig. 1(c). The proof mass' role is to bring the resonant frequency of the resonator close to the frequency of vibration in the environment and to apply a large strain to the piezoelectric film with a small vibration. A polycrystalline Pb(Zr,Ti)O₃ thin film with a thickness of 3 μm was used as the piezoelectric film. The fabrication and electromechanical properties of the resonator are described in Ref. 28.

Figure 1(c) shows the frequency dependencies of the output voltage of the resonator measured by applying sinusoidal vibration with an acceleration of 2 m s⁻². The measurements were conducted by connecting a load resistance of 33 kΩ and using a shaker (PET-01, IMV Corp.) and a lock-in amplifier (LI5640, NF Corp.). The resonator showed a resonant frequency of around 193.2 Hz. The resonance curve slightly tilted toward the low frequency side indicates that the resonator has softening nonlinear characteristics. Analysis using Duffing equation revealed that this resonator has a linear spring constant of 5.3 N m⁻¹ and a nonlinear spring constant of -100 kN m⁻³, respectively. The quality factor, including both electrical and mechanical damping, was determined from the resonance curve to be 220.

3. Results and discussion

For the training and testing of the RC system, vibrations with a frequency of 193.5 Hz and an acceleration of 2 m s⁻² were applied to the resonator. The random time series data with “0” and “1” were prepared, and the amplitude of the acceleration was modulated by the binary input, as shown in Fig. 2(a). The data bit period was 870 ms. The corresponding output waveforms for Nodes A and B are shown in Fig. 2(b). The time constant τ_{CR} for the CR circuit was set at 1 s for this measurement. The simple transient behavior of Node A originates from the resonance of the MEMS resonator. The time constant of the transient behavior was 410 ms. It should be noted that the magnitudes of the output at the input of “1” depend on the previous data. The output is larger when the previous data is “1” and smaller when the previous data is “0”. This response indicates that the RC system used has short-term memory characteristics based on the transient responses. Furthermore, Node B is a delayed signal of Node A by the CR circuit.

The virtual nodes were set up by time-dividing the outputs of Nodes A and B by 1/10 of the data bit period, as shown in Fig. 2(b). In other words, this system has 20 virtual nodes, which are shown as A1, A2, ..., A9, A10, B1, B2, ..., B9, and B10, respectively. Figure 2(c) shows some of the outputs of the virtual nodes generated from the results shown in Fig. 2(b). The output of each virtual node is slightly different, which is an important result for RC.

The computational performance of the piezoelectric MEMS RC system was then evaluated using binary inputs with 1100 continuous steps. To eliminate the influence of the initial conditions of the resonators, the first 100 steps of the

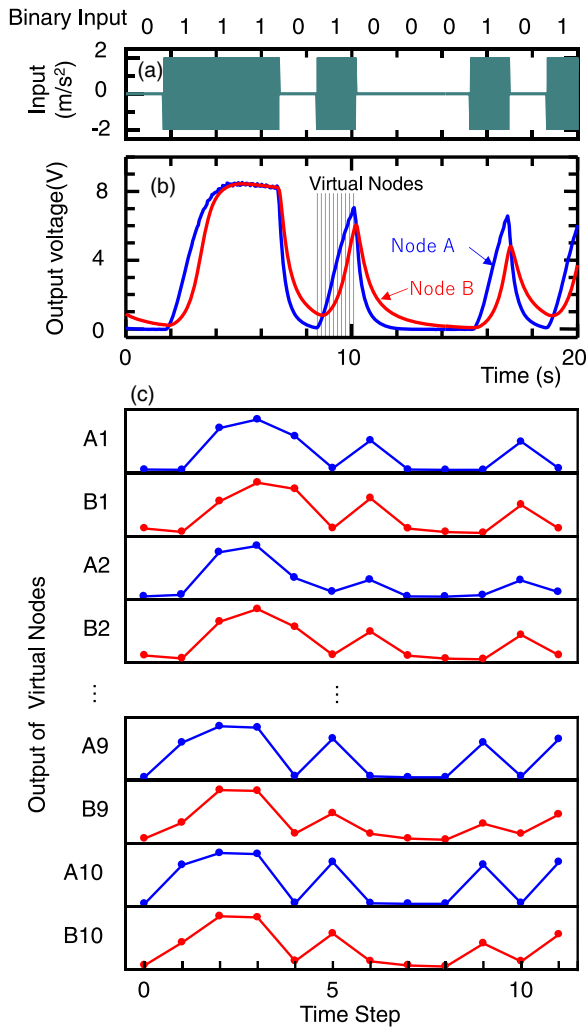


Fig. 2. (a) A waveform of input vibration applied to the resonator. The amplitude of the acceleration was modulated via the binary input shown above. The frequency of vibration was 193.5 Hz. (b) The corresponding output waveforms for Nodes A and B. (c) Outputs of the partially selected virtual nodes.

data were skipped. The remaining 1000 steps were divided into five parts using the k-fold cross-validation method: four datasets were used for training, and one was used for testing. The output of the RC system corresponding to the training

dataset was calculated simply as

$$s(n) = u(n) \cdot W, \tag{1}$$

where $u(n)$ denotes the reservoir states, and W is the weight matrix. W was trained by Ridge regression so that $s(n)$ approximates the target output. RC performance was then tested using W and the test dataset. As in the previous studies, several benchmark tests were conducted.¹⁶⁾ The target data $d(n)$ for short-term memory (STM) tasks is defined by

$$d(n) = v(n - \delta), \tag{2}$$

where n is the time step, δ is the delay step, and $v(n)$ is the binary input data. As the name implies, the STM task examines the short-term memory performance of the system. $d(n)$ for the temporal exclusive OR (XOR) tasks is given by

$$d(n) = v(n) \oplus v(n - \delta), \tag{3}$$

where \oplus is the operator for XOR. Since the result of the exclusive OR is not linearly separable, this task is useful for evaluating the nonlinearity of the system. A more complex task is the parity check (PC) tasks, in which $d(n)$ is given by

$$d(n) = v(n) \oplus v(n - 1) \oplus \dots \oplus v(n - \delta). \tag{4}$$

After correcting the outputs of the RC system for the 1,100 binary inputs, the dataset for the virtual nodes was prepared. Then, the target data for STM, XOR, and PC with different δ were generated, and the weight matrix W was trained for each task. Examples of the benchmark test results are summarized in Fig. 3. The data bit period and τ_{CR} were 870 ms and 1 s, respectively. While δ was changed from 1 to 6, only the results for δ from 1 to 3 are shown in the figure, as the RC system could not predict at high δ . For this evaluation, W was trained by the target data up to 800 time steps, and tests were carried out by the data for the remaining 200 time steps. The figure shows the extracted results for 60 time steps on the boundary. At $\delta = 1$, the target data of XOR and PC tasks were the same, so the test results of the PC task are omitted. For δ up to 2, the RC system predicted the target data well for the three tasks. At $\delta = 3$, there are many parts in which the predicted results were off target.

The squared correlation coefficient r^2 is used to evaluate the level of agreement between the target data and the predicted result is evaluated by the squared correlation

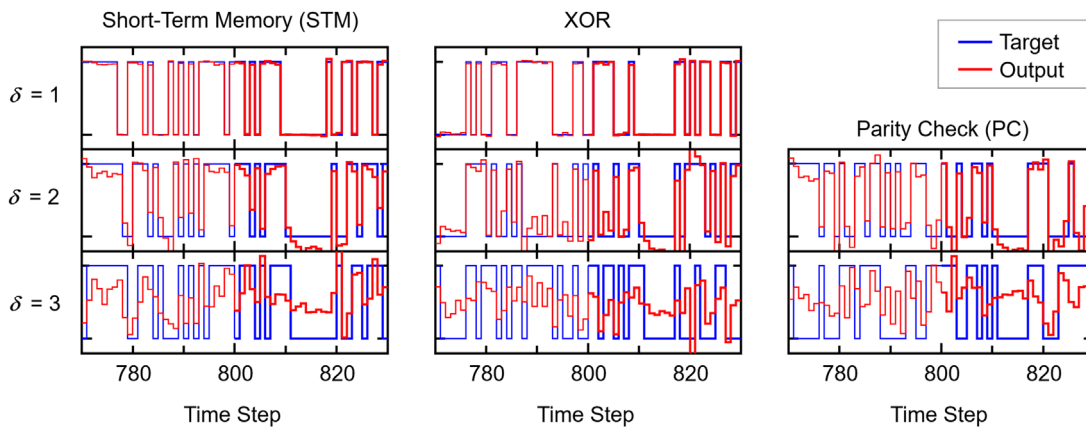


Fig. 3. Target data and the output from the RC system for short-term memory, temporal XOR, and PC tasks at various delay step. Although the training and testing were performed with the data with 1000 steps, only the results for the 60 time steps are shown here. The region below the 800 time step contains the training results, and the region after that contains the testing results.

coefficient r^2 given by¹⁶⁾

$$r^2 = \frac{\sum_n \{(y(n) - \bar{y})(d(n) - \bar{d})\}}{\sqrt{\sum_n (y(n) - \bar{y})^2 \sum_n (d(n) - \bar{d})^2}}, \quad (5)$$

where $y(n)$, \bar{y} , and \bar{d} are the system output, the mean values of $y(n)$ and $d(n)$, respectively. r^2 approaches 1 for good agreements and approaches 0 for disagreements. The dependence of r^2 for the STM, XOR, and PC tasks on δ is shown in Fig. 4. In all tasks, r^2 was larger than 0.9 at $\delta \leq 2$, but dropped to less than 0.5 at $\delta = 3$ and became almost 0 when δ was higher than 3. The difference in r^2 across tasks is small. The performance of the RC system is evaluated using a capacity C defined by¹⁶⁾

$$C = \sum_{\tau=1}^{\infty} r^2(\tau), \quad (6)$$

where $r^2(\tau)$ denotes r^2 at δ for the corresponding task. Using the results of 5-fold cross-validation, C_{STM} was calculated to be 2.23 ± 0.10 , which indicates that the RC system has short-term memory characteristics for 2 time steps. C_{XOR} and C_{PC} , benchmarks for nonlinearity in the system, were 2.08 ± 0.07 , and 2.11 ± 0.10 , respectively. Since short-term memory is also required to perform these nonlinear tasks, it seems reasonable that the three capacity values would be comparable. The results of these three capacities indicate that the piezoelectric MEMS resonator works as a physical RC and is comparable to the results obtained by Si-based RC using a ferroelectric film.¹⁶⁾ On the other hand, the relationship between the nonlinearity of the resonator shown in Fig. 1(c) and the capacities for the nonlinear tasks is not clear at this time. Further study, such as the investigations using resonators with different nonlinearities, is needed to discuss this relationship.

As the RC system in this study used the transient response of the resonators, it can be expected that the data bit period influences the performance. In addition, the effect of τ_{CR} for Node B needs to be investigated. All three benchmark tests were performed comprehensively in various data bit periods and τ_{CR} . Figure 5 shows the dependences of the capacities for the three tasks on the data bit period evaluated at various τ_{CR} . For comparison, we also evaluated them without the CR delay signal. In all tests, the capacities without the CR delay signal were lower than the others. In particular, the difference is remarkable in the STM task. This result indicates that the CR delay signal greatly contributes to improving short-term memory characteristics. Another noteworthy finding is that the capacities for the XOR and PC tests were greatly reduced

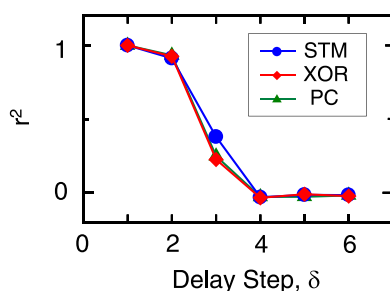


Fig. 4. The squared correlation coefficient r^2 for short-term memory, temporal XOR, and PC tasks as a function of the delay step δ .

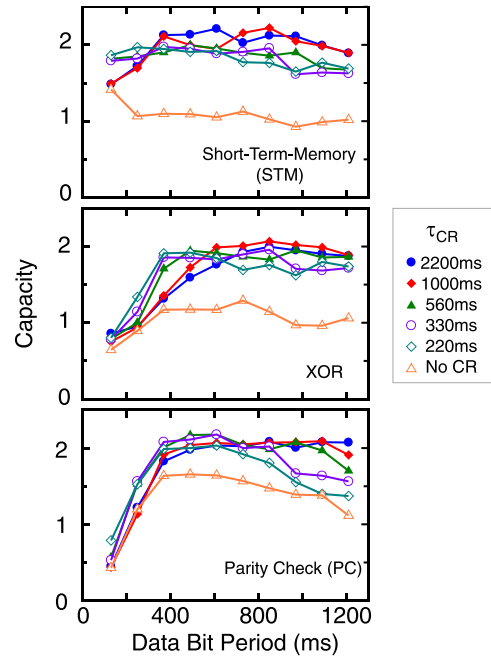


Fig. 5. The capacities for the three tasks' dependencies on the data bit period evaluated at various τ_{CR} .

when the data bit period was lower than the time constant of Node A (410 ms). This result is reasonable, given that transient responses behave linearly below the time constant. On the other hand, the capacities do not depend significantly on the data bit period when the data bit period is larger than the time constant. While the capacities increase slightly with increasing τ_{CR} at the large data bit period region, the effect of τ_{CR} on the capacities is also small.

These results indicate that the RC system has a wide range of conditions for stable operation. While these conditions should be considered critical properties from an application perspective, they seem to imply that small modifications to the reservoir layer do not improve performance. An increase in the number of actual nodes seems to be essential for improving short-term memory characteristics. It is also important to introduce nonlinearity into each node, which requires approaches from both material science and device physics.

4. Conclusions

The nonlinear response in MEMS devices is not favored in current electronics; however, it has become an attractive property in physical RC, which is an emerging piece of edge AI computing technology. In this study, the computational performance of a physical RC system using a piezoelectric MEMS resonator was investigated. Instead of the delayed feedback often used in physical RC, short-term memory characteristics are given to the system by the transient response of the resonator and delayed signal generation by the CR series circuit. The constructed RC system could handle nonlinear tasks that required the memorization of up to two previous datasets. Given that the reservoir layer used consists of only 20 virtual nodes, it can be concluded that piezoelectric MEMS resonators are promising elements for physical RC. The dependencies of the capacities for RC benchmark tests on the data bit period and time constant of the delay signal suggested that the design of the reservoir

layer is essential to improving computational performance. In addition, physical RC is an attractive application field for ferroelectrics, which exhibits nonlinearity not only in piezoelectricity but also in various other properties.

Acknowledgments

This study was supported by the Japan Science and Technology Agency Core Research for Evolutional Science and Technology (JST CREST; Grant No. JPMJCR20Q2 and JPMJCR20C3).

- 1) H. Jaeger and H. Haas, *Science* **304**, 78 (2004).
- 2) G. Tanaka, T. Yamane, J. B. Héroux, R. Nakane, N. Kanazawa, S. Takeda, H. Numata, D. Nakano, and A. Hirose, *Neural Netw.* **115**, 100 (2019).
- 3) K. Nakajima, *Jpn. J. Appl. Phys.* **59**, 060501 (2020).
- 4) S. Kan, K. Nakajima, T. Asai, and M. Akai-Kasaya, *Adv. Sci.* **9**, 2104076 (2021).
- 5) K. Vandoorne, W. Dierckx, B. Schrauwen, D. Verstraeten, R. Baets, P. Bienstman, and J. Van Campenhout, *Opt. Express* **16**, 11182 (2008).
- 6) S. Tsunegi, T. Taniguchi, K. Nakajima, S. Miwa, K. Yakushiji, A. Fukushima, S. Yuasa, and H. Kubota, *Appl. Phys. Lett.* **114**, 164101 (2019).
- 7) A. Z. Stieg, A. V. Avizienis, H. O. Sillin, C. Martin-Olmos, M. Aono, and J. K. Gimzewski, *Adv. Mater.* **24**, 286 (2012).
- 8) C. Du, F. Cai, M. A. Zidan, W. Ma, S. H. Lee, and W. D. Lu, *Nat. Commun.* **8**, 2204 (2017).
- 9) T. Zhang, T. Karaki, and T. Fujii, *Jpn. J. Appl. Phys.* **60**, SFFC05 (2021).
- 10) K. Beppu, F. Funatomi, H. Adachi, and T. Wada, *Jpn. J. Appl. Phys.* **60**, SFFB01 (2021).
- 11) A. Tateyama, Y. Ito, T. Shiraishi, Y. Orino, M. Kurosawa, and H. Funakubo, *Jpn. J. Appl. Phys.* **60**, SFFB03 (2021).
- 12) X. Yuan, Y. Sakurai, S. Kondo, M. Yoshino, T. Nagasaki, and T. Yamada, *Jpn. J. Appl. Phys.* **61**, SN1005 (2022).
- 13) A. Safari, E. K. Akdoğan, and J. D. Leber, *Jpn. J. Appl. Phys.* **61**, SN0801 (2022).
- 14) H. Nam, I. Fujii, S. Kim, T. Ishii, S. Ueno, G. P. Khanal, Y. Kuroiwa, and S. Wada, *Jpn. J. Appl. Phys.* **61**, SN1033 (2022).
- 15) J. Song, Y. Iwamoto, T. Iijima, and S. Okamura, *Jpn. J. Appl. Phys.* **61**, SN1010 (2022).
- 16) K. Toprasertpong, E. Nako, A. Wang, R. Nakane, M. Takenaka, and S. Takaki, *Commun. Eng.* **1**, 21 (2022).
- 17) E. Nako, K. Toprasertpong, R. Nakane, M. Takenaka, and S. Takagi, 2022 IEEE Symp. on VLSI Technology and Circuits, 2022, p. 220, [10.1109/VLSITechnologyandCir46769.2022.9830412](https://doi.org/10.1109/VLSITechnologyandCir46769.2022.9830412).
- 18) E. Nako, K. Toprasertpong, R. Nakane, Z. Wang, Y. Miyatake, M. Takenaka, and S. Takagi, 2020 IEEE Symp. on VLSI Technology, 2020, p. 1, [10.1109/VLSITechnology18217.2020.9265110](https://doi.org/10.1109/VLSITechnology18217.2020.9265110).
- 19) S. Murakami, T. Yoshimura, K. Satoh, K. Wakazono, K. Kariya, and N. Fujimura, *J. Phys. Conf. Ser.* **476**, 012007 (2013).
- 20) M. Aramaki, T. Yoshimura, S. Murakami, K. Satoh, and N. Fujimura, *Sens. Actuators A Phys.* **291**, 167 (2019).
- 21) S. Aphayvong, T. Yoshimura, S. Murakami, K. Kanda, and N. Fujimura, *Jpn. J. Appl. Phys.* **59**, SPPD04 (2020).
- 22) E.-J. Kim, S.-H. Kweon, S. Nahm, Y. Sato, G. Tan, and I. Kanno, *Appl. Phys. Lett.* **121**, 161901 (2022).
- 23) M. Murase, T. Yoshimura, and N. Fujimura, *Jpn. J. Appl. Phys.* **59**, SPPC05 (2020).
- 24) K. Tanaka, Y. Kawata, S. H. Kweon, G. Tan, T. Yoshimura, and I. Kanno, *Appl. Phys. Lett.* **121**, 172901 (2022).
- 25) K. Kariya, T. Yoshimura, S. Murakami, and N. Fujimura, *Jpn. J. Appl. Phys.* **53**, 08NB02 (2014).
- 26) K. Kariya, T. Yoshimura, S. Murakami, and N. Fujimura, *Jpn. J. Appl. Phys.* **53**, 09PA14 (2014).
- 27) M. Aramaki, K. Kariya, T. Yoshimura, S. Murakami, and N. Fujimura, *Jpn. J. Appl. Phys.* **55**, 10TA16 (2016).
- 28) M. Aramaki, K. Izumi, T. Yoshimura, S. Murakami, K. Satoh, K. Kanda, and N. Fujimura, *Jpn. J. Appl. Phys.* **57**, 11UD03 (2018).
- 29) M. Aramaki, T. Yoshimura, S. Murakami, K. Kanda, and N. Fujimura, *Appl. Phys. Lett.* **114**, 133902 (2019).
- 30) S. Aphayvong, S. Murakami, K. Kanda, N. Fujimura, and T. Yoshimura, *Appl. Phys. Lett.* **121**, 172902 (2022).
- 31) G. Dion, S. Mejaouri, and J. Sylvestre, *J. Appl. Phys.* **124**, 152132 (2018).
- 32) B. Barazani, G. Dion, J.-F. Morissette, L. Beaudoin, and J. Sylvestre, *J. Microelectromech. Syst.* **29**, 338 (2020).
- 33) M. H. Hasan, A. Al-Ramini, E. Abdel-Rahman, R. Jafari, and F. Alsaleem, *Sensors* **20**, 6346 (2020).
- 34) T. Zheng, W. Yang, J. Sun, X. Xiong, Z. Wang, Z. Li, and X. Zou, *Sensors* **21**, 2961 (2021).
- 35) J. Sun, W. Yang, T. Zheng, X. Xiong, X. Guo, and X. Zou, *Micromachines* **13**, 317 (2022).
- 36) X. Guo, W. Yang, T. Zheng, J. Sun, X. Xiong, Z. Wang, and X. Zou, *Micromachines* **14**, 161 (2023).
- 37) T. Mizumoto, Y. Hirai, A. Banerjee, and T. Tsuchiya, 2022 IEEE 35th Int. Conf. on Micro Electro Mechanical Systems (MEMS), 2022, p. 487, [10.1109/MEMSS1670.2022.9699777](https://doi.org/10.1109/MEMSS1670.2022.9699777).
- 38) H. Takemura, T. Mizumoto, A. Banerjee, J. Hirotsu, and T. Tsuchiya, 2023 IEEE 36th Int. Conf. on Micro Electro Mechanical Systems (MEMS), 2023, p. 515, [10.1109/MEMS49605.2023.10052286](https://doi.org/10.1109/MEMS49605.2023.10052286).
- 39) J. Sun, W. Yang, T. Zheng, X. Xiong, Y. Liu, Z. Wang, Z. Li, and X. Zou, *Microsyst. Nanoeng.* **7**, 83 (2021).
- 40) T. Yoshimura, T. Haga, N. Fujimura, K. Kanda, and I. Kanno, the 22nd Int. Conf. on Solid-State Sensors, Actuators and Microsystems (Transducers), 2023, p. 457.